High-Efficiency Silicon Solar Cells With Boron Doping in the Back Surface Field via Silicon Paste

Juan Hong, Qidong Geng, Rongwei Xuan, Haibing Huang, and Wei Wang

***Abstract*—In this study, silicon (Si) paste formed by 25-wt% p-type Si nanoparticles and 75-wt% organic solvent is used as a boron (B) source. After conducting a laser opening in the back surface, the preprocessed Si wafers are used as the substrate. The Si paste is then screen-printed above the openings. Finally, B atoms diffuse into Si wafers after being cofired with aluminum paste. The voids in rear local contacts are located by scanning acoustic microscopy. The successful B doping is demonstrated by secondary ion mass spectroscopy. Cells with an average efficiency of over 20% are fabricated on China sunergy's production line, especially with a 0.7% improvement of the fill factor values for passivated emitter and rear contact cells.**

***Index Terms*—Boron doping, screen-printed, Si paste.**

I. Introduction

SILICON (Si) wafer solar cells with an aluminum local back surface field (Al-LBSF) are of great interest due to their low cost and high-efficiency potential for industrial applications [1]–[3]. However, several issues, such as thin p+ layer thicknesses within the contact regions and formation of Kirkendall voids at the rear contact between the Si substrate and the Al rear contact, were observed and reported [4]–[5].

The p+ doping concentration in Al-BSF of Si solar cells is usually about 3×10^{18} atoms/cm^3 or less because of the limited solid solubility of Al in crystalline Si. This doping level cannot generate an adequate inner electric field to decrease the back surface recombination [6]. To obtain concentrations of 10^{19} atoms/cm^3, boron (B) doping is an effective choice to achieve a heavy p+ doping in BSF [7]. Meanwhile, Kirkendall voids as one of the major limiting factors that affect both electrical contact and contact recombination have been reported by numerous researchers [8]–[11]. The voids are believed to occur when the Si diffuses too far into the Al-matrix layer and cannot return to the Al–Si interface before the temperature drops down to the eutectic temperature [3]. Special designed pastes that incorporate some percentage of Si particles must be used to reduce the percentage of Kirkendall voids and increase the thickness of the LBSF [5], [8]. Thus, the preparation of a specific paste that contains both B and Si particles will have great potential for industrial applications.

Recently, numerous attempts have been reported to develop some kinds of paste that include both B and Si. Gao *et al.* [12] introduced a doping source that was B-doped Si nanoparticle (NP)-based Si paste, which can lead to the variation of sheet resistance by changing B concentration. However, the paste had a complex process for preparing B-doped Si NPs. Yuka *et al.* [13] prepared a Si paste via the laser pyrolysis method. The B-doped Si NPs can be produced by using a mixture of silane gas and diborane. All experimental results show that using paste containing B as the doping source is a very feasible method. However, all these abovementioned methods suffer from the same issues, such as high costs and complicated processes for industrial applications. Thus, industrialization has become very difficult.

This study uses the Si paste and screen-printing process as a possible solution to overcome the Kirkendall void formation and realize the localized B doping at the Al–Si interface. Based on China sunergy's passivated emitter and rear contact (PERC) cells' production line, we incorporate fabrication simplifications and industrially applicable processes to develop PERC cells for higher efficiency. After conducting a laser opening in the back surface, the preprocessed Si wafers are used as the substrate. The Si paste is then screen-printed above the openings. Finally, B atoms diffuse into silicon wafers after being cofired with Al paste (Paste RX8254X6, China). Scanning acoustic microscopy (SAM) was used to detect the voids in rear local contacts of PERC and PW-PERC cells. The successful B doping is evidenced by secondary ion mass spectroscopy (SIMS). Cell efficiency was confirmed by the Fraunhofer ISE CalLab. In fact, the good doping performance of Si paste using screen-printing on preprocessed wafers from China Sunergy has been demonstrated [14]. This study shows uniform doping on the BSF and presents further details on the efficacy of Si paste.

II. Experimental Details

A. Silicon Paste Preparation

Si paste formed by p-type Si NPs and an organic solvent is used as the source of B. Si NPs with a diameter of approximately 30 nm are prepared by using the pulsed electrical discharge method. By choosing dopant atoms such as B (p-type) or P (n-type) and concentrations in the raw material, the diffusing performance of NPs can be easily changed. Creating doped films from the Si paste is possible. The p-type preprocessed wafers

Manuscript received January 13, 2016; revised April 30, 2016; accepted May 13, 2016. This work was supported by the Natural Science Foundation of China under Grant 51541505 and Grant 51475236.

J. Hong is with the College of Mechanical Engineering, Yancheng Institute of Technology, Yancheng 224051, China, and also with the College of Mechanical and Electrical Engineering, Nanjing University of Aeronautics and Astronautics, Nanjing 210016, China (e-mail: jameshong@ycit.cn).

Q. Geng and W. Wang are with the College of Mechanical and Electrical Engineering, Nanjing University of Aeronautics and Astronautics, Nanjing 210016, China (e-mail: kengqidong@163.com; wangweinjnuaa@126.com).

R. Xuan and H. Huang are with China Sunergy (Nanjing) PV-Tech Co., Ltd., Nanjing 211100, China (e-mail: rongwei.xuan@chinasunergy.com; haibing.huang@chinasunergy.com).

Color versions of one or more of the figures in this paper are available online at http://ieeexplore.ieee.org.

Digital Object Identifier 10.1109/JPHOTOV.2016.2571630

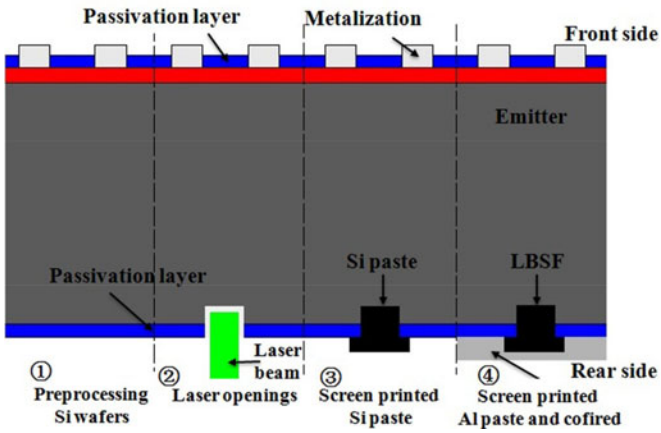

Fig. 1. Process scheme for the PW-PERC cell architecture formation of using Si paste technology.

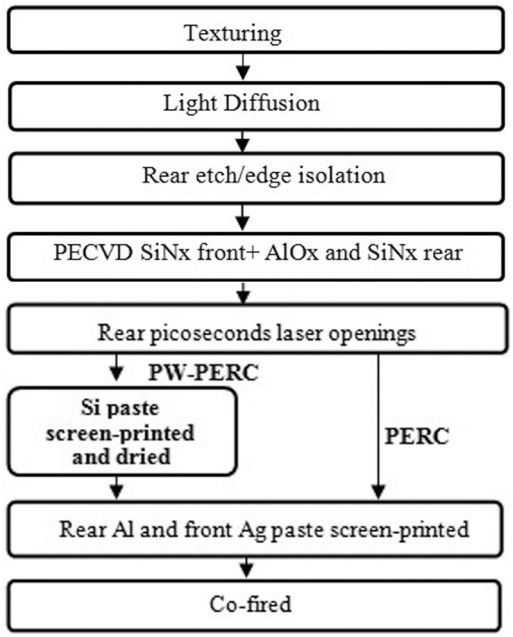

Fig. 2. Process flow diagram for PW-PERC (left) and normal PERC (right) cell fabrication.

from China Sunergy are used as the substrate. After analyzing the printing and diffusing performance of Si paste with different percentages of Si NPs, we chose the Si paste formed by 25 wt% Si NPs for the applications [13].

An advantage of using Si NPs is the reduced melting temperature as compared with bulk Si [15]. The Innovalight's Cougar Process, which uses NPs as source material to prepare Si inks, has confirmed this aspect [16]–[17]. This merit allows the NPs to be cheaply and easily sintered into dense films at low temperatures that do not affect the quality of the bulk wafer. When combined with the Al screen-print firing process, the Si NPs may supplement the Si elements in the Al–Si interface and avoid the Kirkendall void formation in the openings. With the LBSF performed prior to the Al–Si alloying process, cell fabrication with high firing temperatures is possible. If the temperatures are properly increased, then the adequate BSF will be obtained [3].

B. Cell Fabrication

The cell fabrication process was completed on a 35-MW production line by using commercially available silicon wafers. The reference substrates named PW-PERC are made by the following conventional PERC processed steps. Fig. 1 schematically shows the preparation of PW-PERC cells, which has two more steps (screen-printed and dried Si paste) as compared with the normal PERC cells.

The samples were fabricated by using the process flow shown in Fig. 2. The utilized substrates were 180-μm-thick, $156 \times 156\,\text{mm}^2$ pseudosquare, and $1-3\text{-}\Omega\cdot\text{cm}$ Czochralski p-type wafers with surfaces textured with standard upright random pyramids. Following the acidic neutralization in hot hydrochloric acid, the rear side of the wafers received a single-side inline chemical polished in a Si-etchant. After chemical cleaning, the emitter was formed by using $POCl_3$ diffusion in a tube furnace, followed by a phosphorous glass removal in hydrofluoric acid. The emitter sheet resistance after this step was $100 \pm 5\,\Omega/\square$. A 75–85-nm SiN_x layer on the front side was then deposited by plasma-enhanced chemical vapor deposition (PECVD). The rear surface was further passivated by a stack of 5–10 nm of AlO_x and 80–120-nm SiN_x deposited by PECVD. The rear passivation layer is locally opened with a picosecond laser. The openings are a line structure with a pitch ranging from 800 to 1500 μm, and a line width of about 40 μm. All of the above-mentioned steps were processed by using the China Sunergy's production line, which can ensure that the experimental data are more comparable in the same batch. To fabricate PW-PERC cells, the Si paste was self-aligned and screen-printed above the openings. Finally, B atoms diffuse into Si wafers after being cofired with an Al paste (Paste RX8254X6, Wuxi Ruxing Technology Development Co, .Ltd, in China).

The application of SAM by Dressler *et al.* [18] introduced a fast and precise method to detect the voids on a large area without destroying the solar cell. In this paper, SAM was also used to count the number of voids and calculated as a percentage at different cofired temperatures. The solar cell is fixed by small artifacts made from a ferromagnetic material, then submerged in deionized water. The used transducer has a frequency of 150 MHz, resolution of 10 μm, and scanning speed of 2000 mm/s.

The samples were separated into PW-PERC and PERC cells. After the Al paste was screen-printed on the cells, samples were then fired at different cofired temperatures, at the range of $750-900\,^{\circ}\text{C}$ with an interval of 50 °C. That is, each type was divided into four groups for comparison. Every group contained 100 cells. The ten cells, whose efficiencies were near the average level, were selected in each group for testing. After the SAM measurement was carried out on a whole solar cell, the voids were positioned in the thin dark horizontal lines, as seen in Fig. 3, whereas the filled local Si/Al contacts appeared as bright areas. The number of dark lines was counted along the white line on the cell and then calculated as a percentage, with a total of 154 lines. The average percentage of ten cells was used as a statistical result at a cofired temperature.

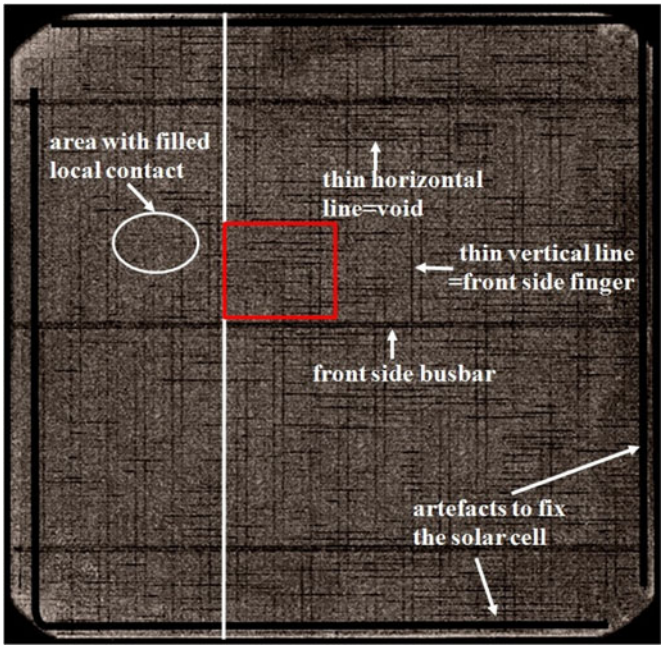

Fig. 3. SAM measurement of a $156 \times 156\,\mathrm{mm}^2$ PW-PERC solar cell cofired at 850 °C. The dark areas along the edge are artifacts to fix the solar cell. Red marker: position for $22 \times 37\,\mathrm{mm}^2$ SAM .White marker: use as a path to indicate the number of thin dark horizontal lines.

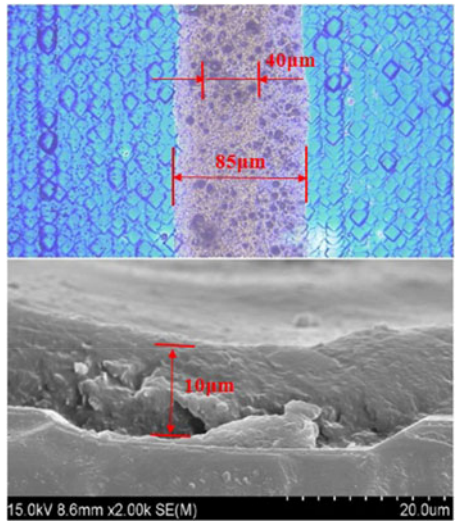

Fig. 4. Process of screen-printed Si paste above the openings. (a) Profile measurement image of a laser microscope of a Si paste finger. (b) SEM images of the finger's cross section.

In calculating the percentage of the voids, the typical microstructure in the filled local contact of PERC and PW-PERC cells on the rear surface can be obtained by scanning electron microscopy (SEM). The feature of eutectic region was also mainly studied. Meanwhile, the difference of the minor element among the Al-matrix, Al–Si alloy, and BSF layers was analyzed by the energy-dispersive spectrometer (EDS). Ten points with adequate LBSF in each cell were selected for research. These points were uniformly sampled from 50 observed points. Finally, ten cells from each high-efficiency group were prepared, and 100 points were studied. The average percentage of minor element among different layers was calculated.

To estimate the thickness of LBSF and calculate the doping depth, the Al and B doping profiles in the filled local contacts of PERC and PW-PERC cells were measured using the SIMS, respectively. Two cells from each group, whose efficiencies were near the average level, were prepared. Five points from each cell with adequate LBSF were first found by SEM and marked for testing. The BSF was then exposed after etching off the sintered Al metal and Al–Si alloy. Finally, the average of doping profile was calculated and compared.

The electrical performance of the PW-PERC cells was characterized to assess the effect of various processed conditions. The cell efficiency reported in this paper was independently verified by the Fraunhofer ISE CalLab, Germany, in accordance with IEC60904, using the 1000-W/m^2 AM1.5 G spectrum at 25 °C. Meanwhile, spectral response ranging from 300 to 1200 nm was measured by employing the filter monochromator, voltage below 0.03 V_{OC}, light at 117 Hz, filters below 15 nm, and temperature at 25 ± 0.5 °C. To further study the device's properties, the cell's internal quantum efficiency (IQE) curve was tested by utilizing PV Measurements QEX10 to compare the carrier absorption and collection at different wavelengths.

III. Results and Discussion

The process of screen-printed Si paste is demonstrated from the results of a profile measurement image of a laser microscope and an SEM image, as shown in Fig. 4. After the preprocessed wafers are prepared, Si paste is screen-printed above the openings on the rear surface, and the dense Si paste fingers are formed, as seen in Fig. 4(a). The line opening width is about 40 μm, whereas the Si paste finger is about 85 μm. The edge of the finger is very clear, and no line bleeding is observed. The cross section of the Si paste finger is shown in Fig. 4(b). After being dried at 350 °C for about 30 s, the thickness of the fingers is about 10 μm. Meanwhile, the thickness uniformity of the finger is seen in the SEM image.

The four edges of a solar cell are fixed on the chuck for testing. After being scanned line by line, SAM measurements are carried out on a $156 \times 156\,\mathrm{mm}^2$ area, as seen in Fig. 3. The thin vertical dark lines are the front-side fingers, whereas the three thick horizontal lines are the front-side busbars. Voids are described as thin dark horizontal lines, whereas filled local Si/Al contacts appear as bright areas (upper right area of the SAM image).

Cells fired at temperatures below 700 °C were not studied because the inadequate thermal treatment led to improperly formed Al contacts. As the temperature rises, Fig. 5 shows that the percentage of the Kirkendall voids in PERC and PW-PERC cells increases as the temperature rises, for the PW-PERC cells less than for the PERC cells. The percentage of the voids in PW-PERC cells is 20% lower than that of PERC cells at 850 °C. This improvement may benefit from the Si paste attached in the local openings beforehand. Normally, as the temperature

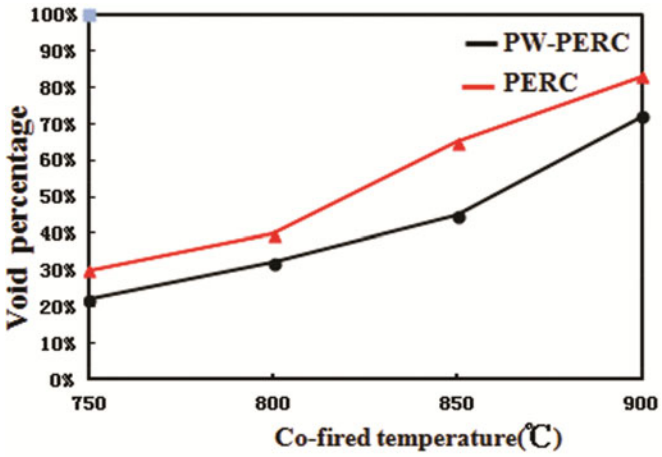

Fig. 5. Comparison of the Kirkendall void percentage of PW-PERC and PERC cells.

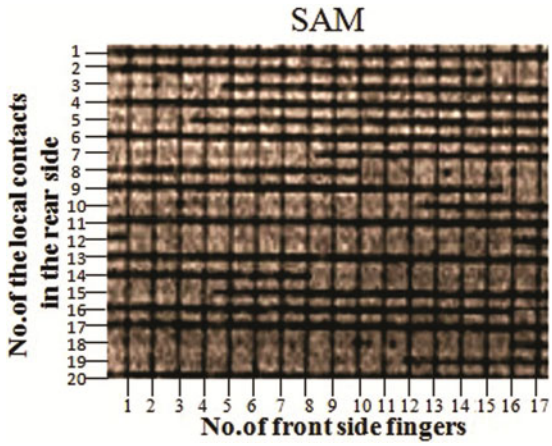

Fig. 6. SAM image of the $22 \times 37\,\mathrm{mm}^2$ area of the PW-PERC solar cell cofired at 850 °C.

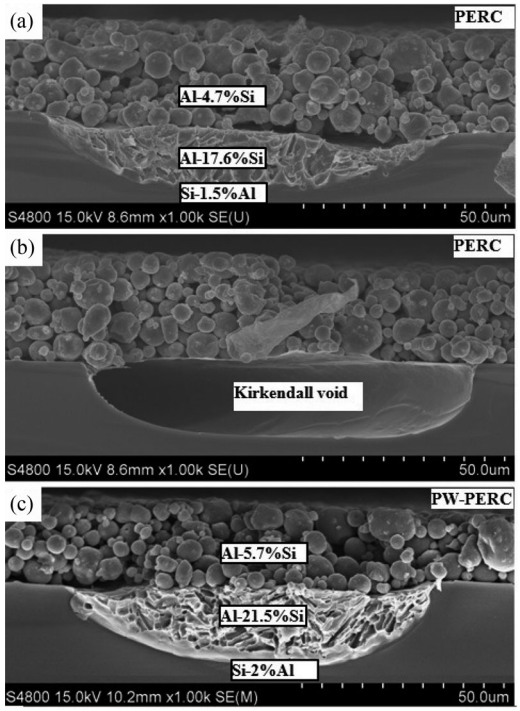

Fig. 7. Cross-sectional SEM images and EDS of (a) the LBSF of PERC, (b) Kirkendall void, and (c) the LBSF of PW-PERC cells.

increases, the Si element diffuses further into the Al-matrix layer and cannot return to the Al–Si interface before the temperature drops down to the eutectic temperature. The predeposited Si paste will supplement the Si element as the Al–Si alloy eutectic formation. As the voids decrease, the electrical contact will be improved, and the fill factor (FF) values will also be mainly benefited.

To obtain a better comparability of void detection, a size of $22 \times 37\,\mathrm{mm}^2$ area (red marker in Fig. 3) is chosen and measured. As seen in Fig. 6, the image shows filled and voids of local contacts, which are collected at the necessary resolution in a reasonable time. The thin vertical lines are the front-side fingers. Twenty thin horizontal lines, which are serially numbered, are the local rear side contacts. Dark lines, which are numbers 1, 2, 4, 6, 9, 11, 13, 14, 16, 17 of the local contact in the rear side, are voids, whereas all other local contacts are filled with eutectic layers. The percentage of the voids in this area is about 50%. In the same way, the average percentage of the voids in a cell is calculated.

Fig. 7(a) shows the cross section of the LBSF of PERC and PW-PERC cells. After being cofired with Al paste at 850 °C, the PERC cells of EDS show that the layers formed after the alloying of Al are the Al-matrix layer in porous state (Al − 4.7%Si), Al–Si alloy eutectic layer (Al − 17.6%Si), and BSF (composition Si − 1.5%Al). By contrast, the PW-PERC cells have very different layer ratios: Al-matrix layer (Al − 5.7%Si), eutectic layer (Al − 21.5%Si), and BSF layer (Si − 2%Al), with each part of the minor element (especially the eutectic layer) significantly increasing.

The Al and B doping profiles in the BSF of PERC and PW-PERC cells were measured by SIMS, respectively. According to this information, we can estimate the thickness of LBSF. After being cofired with Al paste at 750 to 900 °C, the PERC cells of SIMS [see Fig. 8(a)] show that the LBSF thicknesses are 4, 5, 7, and 8 μm, whereas those of the PW-PERC cells [see Fig. 8(b)] are 4, 6, 8, and 9 μm. The Al doping depth in two types of cells at the same cofired temperature is almost the same, but the highest Al concentration in PW-PERC cells (3.5×10^{18} atoms/cm^3 at 900 °C) is higher than that in PERC cells (3×10^{18} atoms/cm^3 at 900 °C).The B atoms are not found in PERC cells. The thickness of the LBSF in PW-PERC cells increases in a reduced amount, but when B dopes into the substrate, the doping concentration increases more. Because of this, the performance of the series resistor (R_s) and open-circuit voltage (V_{oc}) will be improved. When cofired at 900 °C, the highest B concentration reaches about 2.2×10^{19} atoms/cm^3 at the depth of 5–7 μm in the BSF, where the highest Al concentration occurs. The highest B and Al concentration almost appears in the same place, which implies that the B diffusion must be assisted by Al when cofired together.

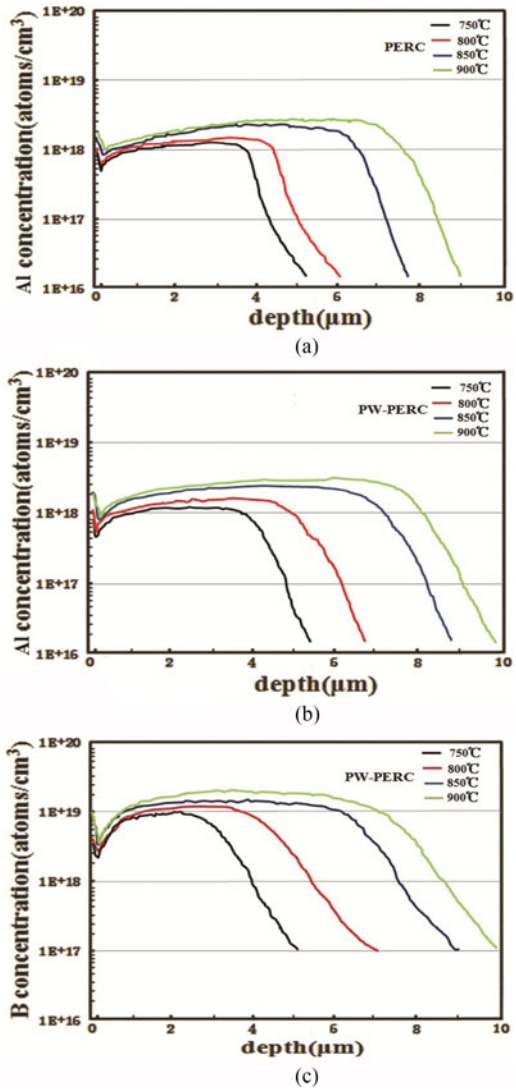

Fig. 8. Comparison of (a) Al doping profiles of PERC cells and (b) Al and (c) B doping profiles of PW-PERC cells in the BSF measured with SIMS, formed at different cofired temperatures.

TABLE I
AVERAGE CELL 1-SUN EFFICIENCIES OF PERC AND PW-PERC CELLS UNDER VARIOUS FIRING CONDITIONS

Cell group	750 °C	800 °C	850 °C	900 °C
PERC(Eff%)	19.3	19.6	19.7	19.5
PW-PERC(Eff%)	19.5	19.8	20	19.6

100 cells each group from one batch of substrate, Eff respective average efficiency, deviation is±0.1.The data were measured in China Sunergy.

A. Solar Cells With Silicon Paste Technology

The average 1-sun efficiencies for all fabricated cells are shown in Table I, which demonstrate that the Kirkendall void percentage and B doping have been significantly affected by the cofired temperature. These trends in the LBSF formation observed in the preceding paragraphs manifested themselves on the solar cell electrical performance. The PW-PERC cells with Si paste resulted in the highest average efficiency of 20% at 850 °C firing, whereas their worst performance (19.5%) was achieved at 750 °C. By contrast, the highest average efficiency of the PERC cells was 19.7% at 850 °C, whereas their worst performance was 19.3% at 750 °C.

Table II shows that the PW-PERC cells have efficiencly improved at all temperatures by using the Si paste technology. The PERC processed at 850 °C achieved a lower Kirkendall void percentage and a higher LBSF depth among all the conditions tested, which was the most promising process condition to obtain high efficiency on the final device. Meanwhile, the PW-PERC cells also achieve the highest efficiency at 850 °C, which agrees well with the SIMS and EDS tests.

To further highlight the performance of the Si paste, the $J-V$ data of the best PW-PERC cells were compared with the best PERC cells made in the same batch of wafers. The summary of this comparison is shown in Table II. Overall, the Si paste technology improves the efficiency of standard PERC cells by about 0.3% at a manufacturing cost similar to that of a local-contact solar cell. A significant part of the improved efficiency for PW-PERC cells was due to a substantial increase of up to 0.7% for the FF of PERC cells, which may be mainly due to the decrease of the voids.

Fig. 9 shows that the independently confirmed best PW-PERC cell *I–V* result verified by the Fraunhofer ISE CalLab in this paper demonstrated the suitability of the PW-PERC solar cell as a production technology that is compatible with a standard China Sunergy 35-MW production line.

Fig. 10 also indicated that the spectral response of the PW-PERC cell was also tested by the Fraunhofer ISE CalLab. This

TABLE II
LIGHT *J–V* DATE OF THE BEST PW-PERC AND PERC CELL

Cell group (Best cell)	V_{oc} (mv)	J_{sc} (mA/cm^2)	FF (%)	Eff (%)	R_s ($\Omega\cdot$cm^2)
PW-PERC	655	39.02	78.9	20.16	0.47
PERC	652	38.65	78.2	19.72	0.55

PW-PERC best cell data confirmed by ISE CalLab in Freiburg, Germany, whereas the PERC cell data were measured in China Sunergy.

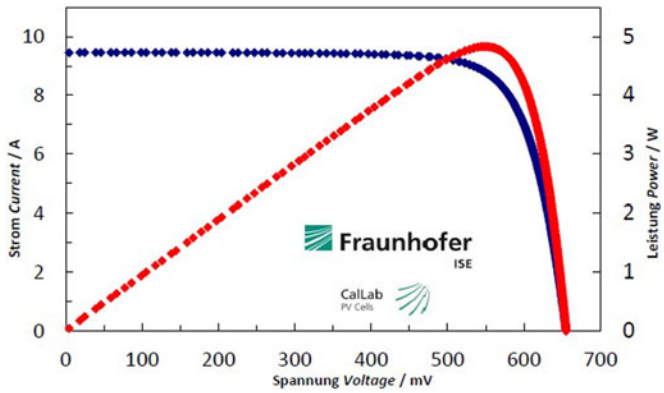

Fig. 9. $I-V$ curve of the PW-PERC production cell measured by Fraunhofer ISE CalLab.

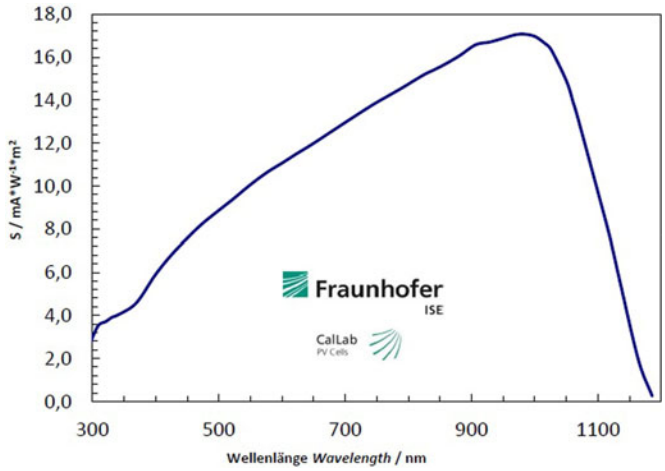

Fig. 10. Spectral response of the PW-PERC production cell measured by Fraunhofer ISE CalLab.

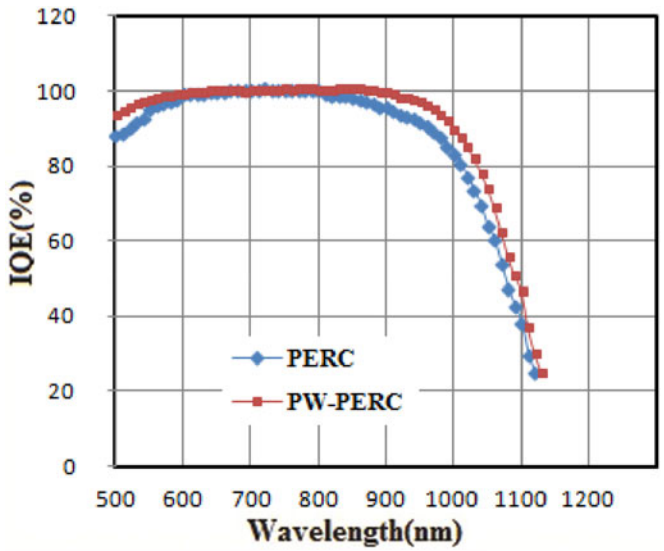

Fig. 11. IQE for best PERC and PW-PERC cell.

curve has direct contact with the short-circuit current density (J_{sc}) of the cells. The peak point appears in the wavelength of 1000 nm, which achieves the highest conversion efficiency of nearly 18 $\text{mA}\cdot\text{W}^{-1}\cdot\text{m}^2$. The curve is relatively flat in the range of 500 − 1000 nm, which means that the J_{sc} of the PW-PERC cells is high and also implies good response characteristics in the long wavelength.

To further distinguish the difference between PERC and PW-PERC, the IQE in the range of 500 − 1200 nm is compared, which is shown in Fig. 11. The said figure clearly shows the difference in the collection of wavelengths of light that are predominately absorbed in the bulk of the wafer and affected by the recombination at the rear contacts. The PW-PERC cells fabricated with B doping obtained higher IQE at all wavelengths. In comparison, PERC cells had a significant drop in IQE in the range of 900–1200 nm, which means that PW-PERC cells have better response characteristics in the long wavelength than PERC cells. The PERC and PW-PERC cells were processed on the same substrate. This difference is believed to be due to the increase of the doping level in the LBSF.

For the fabrication of PW-PERC solar cells on standard production lines, screen-printing can use the existing equipment. Thus, the Si paste technology does not need to add any new equipment. The PW-PERC solar cells follow the same process sequence as conventional PERC solar cells. Minor changes to the existing processes are required, in which the main change is to increase the screen-printing of Si paste on the rear of the device to deposit the B source. This method is simple and applicable in comparison with the traditional spin-on technology.

IV. Conclusion

By delivering the aspects of PERC cells to improve the rear surface design, PW-PERC cells using Si paste and screen-printing achieved an average cell efficiency of 20% in a 35-MW production line, with a highest efficiency of 20.16%. This result translates to a 0.3 − 0.4% improvement in efficiency when directly compared with standard PERC cells. Meanwhile, the Si paste technology can obviously reduce the percentage of Kirkendall voids and increase the doping concentration of the LBSF, which is mainly beneficial to improve the FF and the open-circuit voltage. Verified on industrial-scale equipment using commercially available Si wafers, the Si paste technology may become an economically competitive solar cell manufacturing method in the industry today.

Acknowledgment

The authors would like to thank J. Zhao and J. Lv at China Sunergy for assistance with cells manufacture and measurements.

References

[1] J. Chen *et al.*, "Investigation of screen–printed rear contacts for aluminum local back surface field silicon wafer solar cells," *IEEE J. Photovoltaics*, vol. 3 no. 2, pp. 690–696, Apr. 2013.

[2] Z. Wang *et al.*, "Advanced PERC and PERL production cells with 20.3% record efficiency for standard commercial p-type silicon wafers," *Prog. Photovoltaics, Res. Appl.*, vol. 20, pp. 260–268, 2012.

[3] T. Lauermann, B. Fröhlich, G. Hahn, and B. Terheiden, "Diffusion–based model of local Al back surface field formation for industrial passivated emitter and rear cell solar cells," *Prog. Photovoltaics, Res. Appl.*, vol. 23, pp. 10–18, 2015.

[4] M. Rauer *et al.*, "Aluminum alloying in local contact areas on dielectrically passivated rear surfaces of silicon solar cells," *IEEE Electron. Device Lett.*, vol. 32, no. 7, pp. 916–918, Jul. 2011.

[5] B. Hallam *et al.*, "Record large-area p-type CZ production cell efficiency of 19.3% based on LDSE technology," *IEEE J. Photovoltaics*, vol. 1, no. 1, pp. 43–48, Jul. 2011.

[6] X. Gu, X. Yu, and D. Yang, "Efficiency improvement of crystalline silicon solar cells with a back surface field produced by boron and aluminum co-doping," *Scripta Mater.*, vol. 66, pp. 394–397, 2012.

[7] M. R. Payo *et al.*, "Boron-doped selective silicon epitaxy: High efficiency and process simplification in interdigitated back contact cells," *Prog. Photovoltaics, Res. Appl.*, vol. 22, pp. 711–725, 2014.

[8] D. Lin *et al.*, "Advanced semiconductor finger solar cell with passivated rear and localized contact," in *Proc. 28th Eur. Photovoltaic Sol. Energy Conf. Exhib.*, Paris, France, 2013, pp. 1029–1033.

[9] B. Tjahjono, *et al.*, "Optimizing CELCO cell technology in one year of mass production," in *Proc. 28th Eur. Photovoltaic Sol. Energy Conf. Exhib.*, Paris, France, 2013, pp. 775–779.

[10] D. Chen *et al.*, "Preventing the formation of voids in the rear local contact areas for industrial–type PERC solar cells," in *Proc. 28th Eur. Photovoltaic Sol. Energy Conf. Exhib.,* Paris, France, 2013, pp. 770–774.

[11] R. Horbelta, G. Hahna, R. Jobb, and B. Terheidena, "Void formation on PERC solar cells and their impact on the electrical cell parameters verified by luminescence and scanning acoustic microscope measurements," *Energy Procedia*, vol. 84, pp. 47–55, 2015.

[12] Y. Gao, S. Zhou, and X. Pi, "Doping silicon wafers with boron by use of silicon paste," *J. Mater. Sci. Technol.*, vol. 29, no. 7, pp. 652–654, 2013.

[13] T. Yuka *et al.*, "Laser doping of boron–doped Si paste for high-efficiency silicon solar cells," *Jpn. J. Appl. Phys.*, vol. 54, 2015, Art. no. 08KD06.

[14] J. Hong, W. Wang, B. Shi, and W. Zhang, "Screen–printed Si paste to form efficient B doping in a back surface field," *IEEE Electron Device Lett.*, vol. 36, no. 1, pp. 8–10, Jan. 2015.

[15] A. N. Goldstein, "The melting of silicon nanocrystals: Submicron thin-film structures derived from nanocrystal precursors, " *Appl. Phys. A*, vol. 62, pp. 33–37, 1996.

[16] K. Alberi *et al.*, "Localized doping using silicon ink technology for high efficiency solar cells," in *Proc. IEEE Photovoltaic Spec. Conf.*, 2010, pp. 001465–001469.

[17] H. Antoniadis, "Silicon ink high efficiency solar cells," in *Proc. 34th IEEE Photovoltaic Spec. Conf.*, 2009, pp. 650–654.

[18] K. Dressler *et al.*, "Nondestructive characterization of voids in rear local contacts of PERC type solar cells," *IEEE J. Photovoltaics*, vol. 5, no. 1, pp. 70–76, Jan. 2015.

Authors' photographs and biographies not available at the time of publication.